0.1 Interplay between the Geometrical and the Electronic Structure in Quasicrystals

J. Kroha, D. Walther, and R. v. Baltz

Institut für Theorie der Kondensierten Materie
Universität Karlsruhe
D-76128 Karlsruhe
Germany

0.1.1 Introduction

The very existence of a quasicrystalline state of matter, which was first discovered by Shechtman *et al.* [1] in 1984 and has since been found in an abundance of compounds, poses two intellectual challenges. (1) What are the microscopic mechanisms that make the atoms form a highly ordered, yet not translationally invariant, quasiperiodic state; and (2) what is the nature of the quantum states of electrons moving on a quasicrystalline lattice? Soon after their discovery it became clear that in quasicrystals (QC) there is an intimate relationship between the geometrical arrangement of the ions and the electronic properties.

QC and their periodic approximants exhibit unusual electronic structure and transport properties, e.g. a pronounced pseudogap at the Fermi level ε_F and an extremely low or even vanishing electrical conductivity, compared to the conductivity of their metallic constituents. It is generally believed that these anomalies are directly related to the long–range but aperiodic order. For an introduction and for reviews of the physical properties of QC see Ref. [2] and Refs. [3, 4], respectively, whereas the most recent progress of our understanding is documented in Ref. [5]. Both the nature of the electron density of states (DOS) and of the wave functions, delocalized or critical (power-law localized) have remained controversial up to now. In some QCs the low conductivity seems to be associated with the pseudogap in the DOS rather than with a short mean free path or even localization of the wave function [6]. This interpretation is consistent with the frequency dependence of the conductivity [3, 7]. The spiky structure of the DOS, predicted by previous two– and three–dimensional calculations [8], has not been observed experimentally [9] and might be a numerical artifact [10].

The formation of a QC is, in turn, strongly influenced by the electron system. The QC phase is stable only in a small window of oncentrations of the elemental constituents in which the average atomic spacing coincides with the wave length of the electronic Friedel charge density oscillations. Moreover, momentum space (electron diffraction) [12] as well as real space (z-contrast electron microscopy) [13] probes of QCs reveal a concentrical, shell–like arrangement of the ions, similar to the amorphous phase [11, 12]. Hence, the Hume–Rothery stabilization mechanism [14] should play an important role in the formation of QCs, i.e. the ions are bound in the minima of the Friedel potential around an arbitrary central ion, and the electron system minimizes its energy by forming a pseudogap at the Fermi level ε_F. In addition, an entropic stabilization mechanism has been put forward [15], relevant for aperiodic random tilings.

Electronic structure and transport calculations in QCs have been hampered by the absence of translational symmetry and, hence, by the invalidity of Bloch's theorem. When describing

the electronic properties on a QC lattice one has to bear in mind that the electrons can feel the long–range aperiodic order only over a distance given by their phase coherence length $\ell_\phi = v_F \tau_\phi$, with v_F the Fermi velocity and τ_ϕ the phase coherence time. Hence, those properties originating from the aperiodic order, e.g. the spikyness of the DOS in one dimension, will gradually emerge as the temperature T is lowered and τ_ϕ diverges, the energy resolution of these features given by $\hbar/\tau_\phi$. In order to describe these structures one must use mathematical methods that incorporate the QC order exactly [16] or use periodic approximants. On the other hand, when ℓ_ϕ is only of the size of a few concentrical atom clusters, self–averaging takes place, and, despite of perfect QC order, the electron feels an effective random potential, with the individual scattering potential provided by a concentrical cluster within the QC. Especially in this regime electron–electron interactions may become important.

According to these two cases, in this project we study in this project (1) the electronic structure and electrical conductivity of one–dimensional QCs in the $T = 0$ limit using a newly developed, exact path renormalization scheme [17, 18], and (2) the stability of QC phases and interaction–induced correlation effects at elevated temperature within the Hume–Rothery mechanism in analogy to amorphous metals [19, 20].

0.1.2 Electronic Structure and Conductivity of Fibonacci Chains

One–dimensional QCs, such as the Fibonacci chain (FC), have been studied in great detail by many researchers, because analytical treatments and exact results are possible. The most striking feature of this model is that quasiperiodicity induces long range correlations giving rise to an 'intermediate' or 'critical' state of localization, while all states are localized in randomly disordered systems in one dimension. The so–called 'critical states' are associated with singular continuous spectra of the Hamiltonian [4].

An important step towards the understanding of the electronic structure of one–dimensional QCs was made by Iguchi [21] and later on by Kramer [22] and Baake *et al.* [23] who recognized the importance of the automorphism group $\mathbf{\Phi}_n$ of free groups which was discovered by Nielsen [24] a long time ago. Most progress in investigating 1D models has been made by methods based upon the trace map and real–space decimation techniques to investigate the dynamical properties of the traces which, however, do not exploit on the full structure of automorphism group. The situation is different for local properties such as the local density of states or for wave–functions. In a previous article [17] we developed a real space renormalization scheme which is based upon a real–space rescaling procedure of the Dyson equation for one–band tight–binding models of generalized Fibonacci chains. Herein, we presented an approach for finding all possible successions of given elementary rescaling transformations to calculate the diagonal elements of the Green's function and, hence, for the local density of states at site μ

$$\rho_\mu(E) = -\frac{1}{\pi}\Im m G_{\mu\mu}(E + \imath\eta), \quad \eta \to 0^+. \tag{1}$$

Later on, we were able to generalize this method to include the non–diagonal elements $G_{\mu\nu}(E)$ for all sites μ, ν [25] and to set up a renormalization scheme for the conductivity itself [26]. Previously, no renormalization treatments of the complete Green's function have been known and calculations for the (dc) conductivity were fully numerical [27, 28, 29].

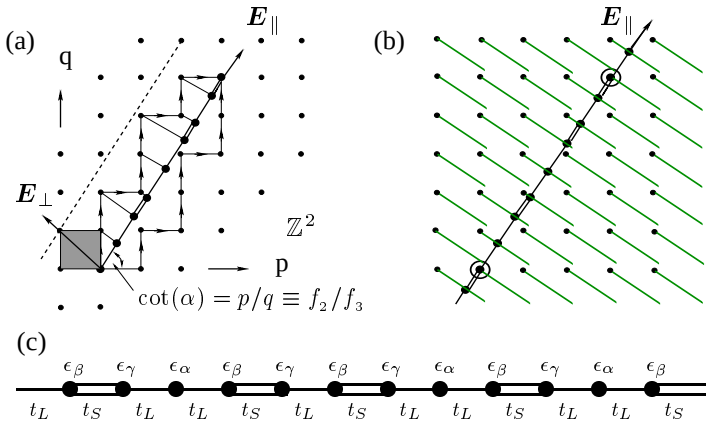

Figure 1: Fifth generation standard Fibonacci lattice $w_5 = LSLLSLSLL\,SLLS$ corresponding to a supercell with $f_5 = 13$ atoms. (a) Strip–projection scheme, (b) cut method for generating the quasiperiodic structure (c), $LSLLSLSLLSLLS$ [2].

A. Generating algorithms for Fibonacci chains

For simplicity, we will discuss in this article only the case of the standard FC which is specified by two different types of bonds denoted by L ("long") and S ("short"), see Fig. 1. One may describe the geometric structure of such lattices by *words* $w(L,S)$, i.e. strings in the symbols L, S representing the corresponding linear arrangement of the "letters" L and S. These words can be generated by an (infinite) repetition of the recursion law (Nielsen transformation (NT))

$$w_n = w_{n-2} * w_{n-1}, \qquad w_{-1} = S, \quad w_0 = L\,, \tag{2}$$

where the symbol $*$ is defined as the concatenation of two strings and $n = 1, 2, \ldots$ The length of the FC in the n^{th} generation, $|w_n| = f_n$, i.e. the number of letters in $w_n(L,S)$, satisfies the recursion relation for the Fibonacci numbers [30]

$$f_n = f_{n-1} + f_{n-2}, \qquad f_{-1} = f_0 = 1\,. \tag{3}$$

Alternatively, the n^{th} order approximants can be generated by substitutions (morphisms), which operate on the symbols L, S rather than on words $w_n(L,S)$

$$\boldsymbol{\mathcal{L}}: \begin{cases} L \mapsto LS \\ S \mapsto L \end{cases} . \tag{4}$$

The mapping $\boldsymbol{\mathcal{L}}$ may be viewed as the *orbit* of L, i.e. $w_n = \boldsymbol{\mathcal{L}}^n(L)$:

$$L \overset{\boldsymbol{\mathcal{L}}}{\longmapsto} LS \overset{\boldsymbol{\mathcal{L}}}{\longmapsto} LSL \overset{\boldsymbol{\mathcal{L}}}{\longmapsto} LSLLS \overset{\boldsymbol{\mathcal{L}}}{\longmapsto} \ldots \overset{\boldsymbol{\mathcal{L}}}{\longmapsto} LSLLSLSLLSLLS\cdots\,.$$

B. Electronic Structure and Path Renormalization

In our study we employ the following tight–binding Hamiltonian

$$\hat{\boldsymbol{\mathcal{H}}}[\boldsymbol{\epsilon},\boldsymbol{t}] = \sum_{\mu} |\mu > \epsilon_{\mu} < \mu| \; + \; \sum_{\mu\nu} |\mu > t_{\mu\nu} < \nu| \, , \qquad t_{\mu\nu} = t_{\mu\pm}\delta_{\mu\pm 1,\nu} \tag{5}$$

where $|\mu>$ is a Wannier state centered at site $\mu \in \boldsymbol{G} = [-M, N-1] \subseteq \mathbb{Z}$, and the real $\epsilon_{\mu}, t_{\mu\nu}$ denote the site–energies and the nearest–neighbour transfer integrals, respectively. ($t_{\mu\nu} > 0$). The FC has the speciality that there is no S–S bonding, hence only three of the possible four combinations occur,

$$\epsilon_{\mu} = \begin{cases} \epsilon_{\alpha} & : \quad t_{\mu-1,\mu} = t_{\mu,\mu+1} = t_L \\ \epsilon_{\beta} & : \quad t_{\mu-1,\mu} = t_L, \; t_{\mu,\mu+1} = t_S \\ \epsilon_{\gamma} & : \quad t_{\mu-1,\mu} = t_S, \; t_{\mu,\mu+1} = t_L \, . \end{cases} \tag{6}$$

Thus, in this case we set $\boldsymbol{\epsilon} := (\epsilon_{\alpha}, \epsilon_{\beta}, \epsilon_{\gamma})$ and $\boldsymbol{t} := (t_L, t_S)$, respectively. To each word $w = (y_{\mu})_{\mu\in G} \equiv y_{-M} y_{-M+1} \cdots y_{N}$, with $y_{\mu} \in \{L, S\}$, $M + N \geq 2$, we uniquely assign a *dual word* $\Sigma_w = (\sigma_{\mu})_{\mu=-M}^{N-1} \equiv (\sigma_{-M}, \ldots, \sigma_{N-1})$, where each symbol $\sigma_{\mu} \in \{\alpha, \beta, \gamma\}$ will be related to the pair $(y_{\mu}, y_{\mu+1})$ by the map $(LL, LS, SL) \leftrightarrow (\alpha, \beta, \gamma)$. For example, the dual word pertaining to w_5 is $\Sigma_{w_5} = \gamma\beta\gamma\alpha\beta\gamma\beta\gamma\alpha\beta\gamma\alpha$, see Fig. 1. Let $\Sigma_u = (\sigma_{\mu}^{u})_{\mu=-m}^{n-1}$ and $\Sigma_v = (\sigma_{\mu}^{v})_{\mu=-p}^{q-1}$ be the dual words of u, and v respectively. We define the product of two dual words, corresponding to the product $w = u * v$, by $\Sigma_u \wedge \Sigma_v =: \Sigma_w$, with $\Sigma_w = (\sigma_{-m}^{u}, \cdots \sigma_{n-1}^{u}, \sigma_n, \sigma_{-p}^{v}, \cdots \sigma_{q-1}^{v})$, $\sigma_n := (y_n^u, y_{-p}^v)$, where y_n^u (y_{-p}^v) is the last (first) letter of u (v).

To set up a renormalization scheme we approximate the aperiodic FC by a periodic approximant of length $2N$ ($M = N$),

$$\Sigma^{G} = \underbrace{\Sigma_n \wedge \Sigma_n \wedge \ldots \wedge \Sigma_n}_{2N' \text{times}} , \quad \boldsymbol{G} = [-N, N-1], \;\; N = N' f_{n} \, , \tag{7}$$

where $f_{n} - 1$ denotes the number of symbols σ_{μ} in Σ_n, and we have the periodicity $\epsilon_{\mu+f_n} = \epsilon_{\mu}$, $t_{\mu\pm+f_n} = t_{\mu\pm}$. $\mu = \tilde{\mu} + m f_{n}$ with $\tilde{\mu} \in [0, f_{n} - 1]$ labels the atoms inside the Fibonacci supercell, and $m \in [-N', N' - 1]$ labels the vectors of the Bravais lattice of the periodic approximant. Obviously, there is a unique correspondence between the dual word Σ and the FC Hamiltonian $\hat{\boldsymbol{\mathcal{H}}}_{\Sigma}[\boldsymbol{\epsilon}, \boldsymbol{t}]$.

In site representation, the eigenstates of Eq. (5) can be represented in terms of the two fundamental solutions $\{\mathcal{P}_{\mu}\}$ and $\{\mathcal{Q}_{\mu}\}$ of the discrete Schrödinger equation

$$\left(\hat{\boldsymbol{\mathcal{H}}}_{\Sigma_n}[\boldsymbol{\epsilon}, \boldsymbol{t}] \, \Psi\right)_{\mu} := t_{\mu+} \, \Psi_{\mu+1}(E) + t_{\mu-} \, \Psi_{\mu-1}(E) + \epsilon_{\mu} \Psi_{\mu}(E) = E \, \Psi_{\mu}(E) \, , \tag{8}$$

such that the (unnormalized) solutions are

$$\Psi_{\mu}^{\pm}(E) := \mathcal{P}_{\mu}(E) + m_{\pm}(E) \mathcal{Q}_{\mu}(E) \, . \tag{9}$$

$\mathcal{P}_{\mu}(E)$, $\mathcal{Q}_{\mu}(E)$, respectively, denote polynomials of degree $\mu - 1$ and μ with initial conditions $\mathcal{P}_{-1} = -1/t_{0}$, $\mathcal{P}_{0} = 1$ and $\mathcal{Q}_{-1} = 0$, $\mathcal{Q}_{0} = 1/t_{0}$ [31]. In addition, we have to fulfill the Bloch

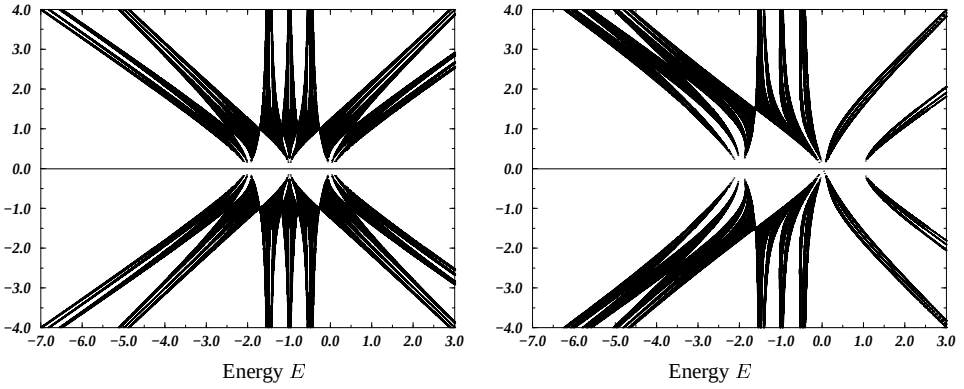

Figure 2: Energy spectrum of the standard Fibonacci chain in dependence of the hopping parameter $t_{_L}$ (y axis). Energy units are chosen such that $t_{_S} = 1$ throughout this chapter. Left panel: constant onsite energies $\epsilon_\mu = 1$. Right panel: $\epsilon_\alpha = -\epsilon_\beta = \epsilon_\gamma = 1$.

conditions $\Psi_{\mu\pm f_{_n}} = \exp(\pm\imath k a)\Psi_\mu$, where $a = f_{_n}$ is the lattice constant and $k = k(E)$ is the wave vector. According to time reversal symmetry a state of energy E is twofold degenerate which will be denoted by $|E,\pm\rangle$ and $\Psi^\pm_\mu(E) = \langle\mu|\pm\rangle$, respectively. $m_\pm(E)$ denotes the Titchmarsh–Weyl function [32]

$$m_\pm(E) \;=\; \frac{e^{\pm ik(E)f_{_n}} + t_{_0}\mathcal{P}_{f_{_n-1}}(E)}{t_{_0}\mathcal{Q}_{f_{_n-1}}(E)}\,, \tag{10}$$

$$e^{\pm ik(E)f_{_n}} \;=\; \frac{\Delta_{f_{_n}}}{2} \pm \sqrt{\left(\frac{\Delta_{f_{_n}}}{2}\right)^2 - 1}\,, \qquad \Delta_{f_{_n}} = t_{_0}(\mathcal{Q}_{f_{_n}} - \mathcal{P}_{f_{_n-1}})\,, \tag{11}$$

where $f_{_n}k(E) = (p\pi)/N' = \arccos\big(\Delta_{f_{_n}}(E)/2\big) \in [0,\pi)$, and $0 \le p < N'$. For the standard one-atomic tight–binding chain with equal $t's$ and $\epsilon's$ $\Delta_{f_{_n}}(E)$ and $\mathcal{Q}_\mu(E) = \mathcal{P}_{\mu-1}$ are, apart from a scale factor, Chebyshev polynomials $T_\mu(x)$, $U_\mu(x)$ of first and second kind, respectively [33]. $\Psi^\pm_\mu(E) = e^{\pm\imath\mu k}$, $E(k) = \epsilon - 2t\cos(k)$. The central quantity of our interest is the resolvent of the Hamiltonian Eq. (5) with kernel

$$G_{\mu\nu}(z) = \frac{1}{W(z)}\big(\Theta_{\mu-\nu}\Psi^+_\mu\Psi^-_\nu + \Theta_{\nu-\mu}\Psi^-_\mu\Psi^+_\nu\big), \tag{12}$$

the Wronskian $W(z) = t_{\nu+1}(\Psi^+_\nu\Psi^-_{\nu+1} - \Psi^+_{\nu+1}\Psi^-_\nu)$ and the discrete step function $\Theta_{_\mu} = 1$ if $\mu \ge 1$ and $\Theta_{_\mu} = 0$ else. From Eq. (12) one immediately obtains the local density of states (LDOS), Eq. (1), and the total DOS $\mathcal{N}(E) = \sum_\mu \rho_\mu(E)$. The former is related to the wave function by $\rho_\mu(E) = |\Psi_\mu|^2$, while the support of the latter is simply the electronic spectrum $\sigma(\hat{\boldsymbol{\mathcal{H}}})$ of the Hamiltonian. Numerical examples for the spectrum and the LDOS are displayed in Figs. 2,3. Note that the symmetry of the electronic spectrum $\sigma(\hat{\boldsymbol{\mathcal{H}}}[\boldsymbol{\epsilon},\boldsymbol{t}]) = \mathrm{supp}(\mathcal{N}(E))$, as a function of the hopping energy $t_{_L}$, with respect to $t_{_L} = 0$ is typical for all two–letter

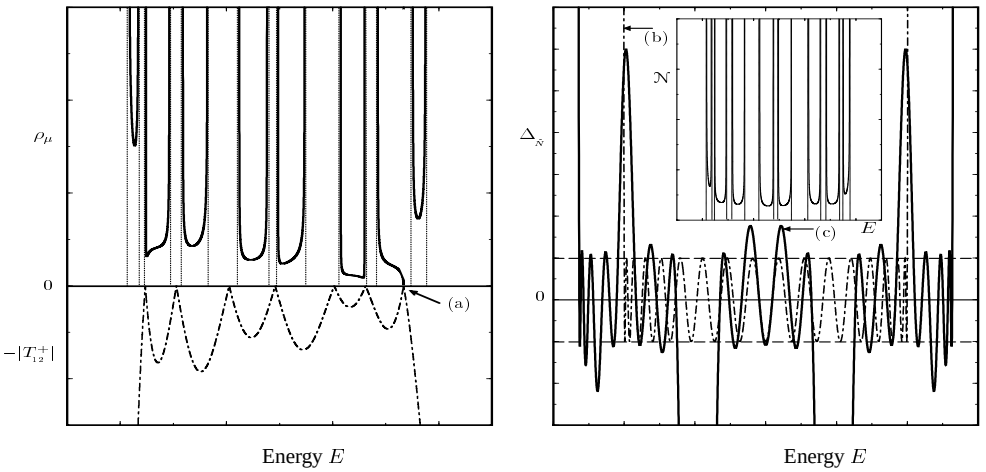

Figure 3: Local density of states $\rho_\mu(E)$ (left) and the trace Δ_{f_n} (right) as functions of energy at site $\mu = 888$ for the FC lattice w_{15}. The square root singularities at the mini–band edges are a consequence if the periodic boundary conditions of the approximant. For further details see text.

chains irrespective of the generating algorithm. There is a trivial gap–closing for $t_L = t_S = 1$ in the case of the diagonal model (i.e. all $\epsilon_\mu = \epsilon$). This situation changes, however, in the non–diagonal case (right section of Fig. 2). Since the point spectrum is empty in the case of the FC, the spectrum is determined by $\sigma(\hat{\boldsymbol{\mathcal{H}}}) = \{E \in \ ||\Delta_{f_n}| \leq 2\}$. In the right section of Fig. 3 the two possibilities ((b) $t_L = t_S$, and (c) $t_L \neq t_S$) are shown. The zeros of the renormalized hopping energies $T_{12}^+ := 1/t_L^*$ are located in the gaps, thus the LDOS usually (but not always, cf. arrow (a) in the left section of Fig. 3) vanishes only in the cases when gap–closing takes place (cf. left panel of Fig. 3).

For large approximants a direct solution is intractable. The idea of path renormalization is to decimate a given FC Σ^G and its corresponding Hamiltonian $\hat{\boldsymbol{\mathcal{H}}}_\Sigma$ and Green's function G by means of a deflation operation such that G is invariant on the remaining sites. The deflation is successively repeated until a tractable cell size (a simple periodic lattice) is reached. As an example, we demonstrate how to calculate the LDOS $\rho_\mu(E)$. The starting point is observed by constructing to any inverse substitution $\boldsymbol{\mathcal{M}}^{-1}$ a suitable decimation transformation $\overline{\boldsymbol{\mathcal{M}}}^{-1}$ which splits a given lattice (chain) $\mathcal{L}$ into two pieces $\mathcal{L}_1 \cup \mathcal{L}_2$, where $\mathcal{L}_2$ corresponds to the vertices which are eliminated, and the lattice $\mathcal{L}_1$ consists of the vertices which survive this elimination. In case of the FC we can confine ourselves to the purely positive deflations, for the general case see Ref. [18]. One can show that all possible deflations are compositions of the two elementary deflations $\overline{\boldsymbol{\mathcal{L}}}^{-1} : LS \to L$, $L \to S$, and $\overline{\boldsymbol{\mathcal{R}}}^{-1} : SL \to L$, $L \to S$, respectively. From a mathematical point of view one describes any such decimation $\overline{\boldsymbol{\mathcal{M}}}^{-1}$ by

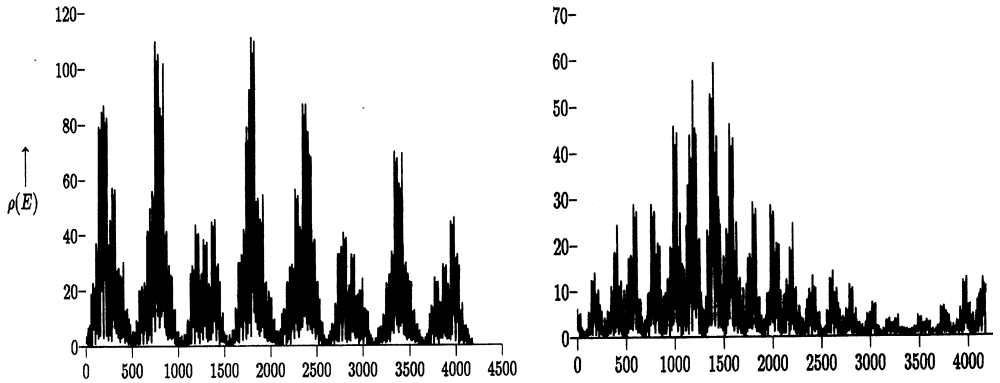

Figure 4: Local density of States as a function of site index for two different energies (a) $E = 2.791$ and (b) $E = 2.759$. $f_{17} = 4181$. $\epsilon_\alpha = -\epsilon_\beta = \epsilon_\gamma = 1$ and $t_{_L} = 1,\ t_{_S} = 1.5$.

the projections

$$\hat{\mathcal{P}}_1^{\mathcal{M}} := \sum_{\alpha\in\mathcal{L}_1} |\alpha\rangle\langle\mu|, \quad \hat{\mathcal{P}}_2^{\mathcal{M}} := \sum_{\beta\in\mathcal{L}_2} |\beta\rangle\langle\mu| = \mathbb{1} - \hat{\mathcal{P}}_1^{\mathcal{M}}, \tag{13}$$

implying the partition $\ell_2(\mathcal{L}) = \ell_2(\mathcal{L}_1) \oplus \ell_2(\mathcal{L}_2)$ of the Hilbert space and of the Dyson equation

$$\begin{pmatrix} z-\hat{\mathcal{H}}_{11} & \hat{\mathcal{H}}_{12} \\ \hat{\mathcal{H}}_{21} & z-\hat{\mathcal{H}}_{22} \end{pmatrix} \begin{pmatrix} \hat{\mathcal{G}}_{11} & \hat{\mathcal{G}}_{12} \\ \hat{\mathcal{G}}_{21} & \hat{\mathcal{G}}_{22} \end{pmatrix} = \begin{pmatrix} \mathbb{1}_1 & \mathbf{0} \\ \mathbf{0} & \mathbb{1}_2 \end{pmatrix}, \tag{14}$$

where we have set $\hat{\mathcal{H}}_{ij} = \hat{\mathcal{P}}_i^{\mathcal{M}}\hat{\mathcal{H}}\hat{\mathcal{P}}_j^{\mathcal{M}}$, and $\hat{\mathcal{G}}_{ij} = \hat{\mathcal{P}}_i^{\mathcal{M}}\hat{\mathcal{G}}\hat{\mathcal{P}}_j^{\mathcal{M}}$, respectively. In order to calculate observable quantities we are interested in the Green's function, rather than in the Hamiltonian, for the *new* lattice $\mathcal{L}_1$, i.e.

$$\hat{\mathcal{G}}_{11}(z) = \hat{\mathcal{P}}_1\hat{\mathcal{G}}(z)\hat{\mathcal{P}}_1 =: {}^{R}\hat{\mathcal{M}}^{-1}\cdot\hat{\mathcal{G}}(z). \tag{15}$$

We introduce here the "super operator" ${}^{R}\hat{\mathcal{M}}^{-1}$ acting in the space of Green's functions, which is induced by the deflation $\overline{\mathcal{M}}^{-1}$ of the FC. The superscript "R" is reminiscent of renormalization. From Eq. (14) one immediately obtains a new Dyson equation

$$\begin{aligned} &\hat{\mathcal{G}}_{11} = \hat{\mathcal{G}}_{11}^{(0)}(\mathbb{1} + \hat{\mathcal{V}}\hat{\mathcal{G}}_{11}) \\ &\hat{\mathcal{G}}_{11}^{(0)} := (z-\hat{\mathcal{H}}_{11})^{-1},\ \hat{\mathcal{V}} := \hat{\mathcal{H}}_{12}(z-\hat{\mathcal{H}}_{22})^{-1}\hat{\mathcal{H}}_{21}. \end{aligned} \tag{16}$$

$\hat{\mathcal{G}}_{11}$ is the resolvent of the new effective Hamiltonian $\hat{\mathcal{H}}^{\text{eff}}[z] := {}^{R}\hat{\mathcal{M}}^{-1}\cdot\hat{\mathcal{H}}$, where

$$\hat{\mathcal{H}}^{\text{eff}}[z] := \hat{\mathcal{H}}_{11} + \hat{\mathcal{H}}_{12}\frac{1}{z-\hat{\mathcal{H}}_{22}}\hat{\mathcal{H}}_{21} = \sum_{\mu,\nu\in\mathcal{L}_1} (\mathcal{H}_{|\mathcal{M}}[z])_{\mu\nu}\,|\mu\rangle\langle\nu| \tag{17}$$

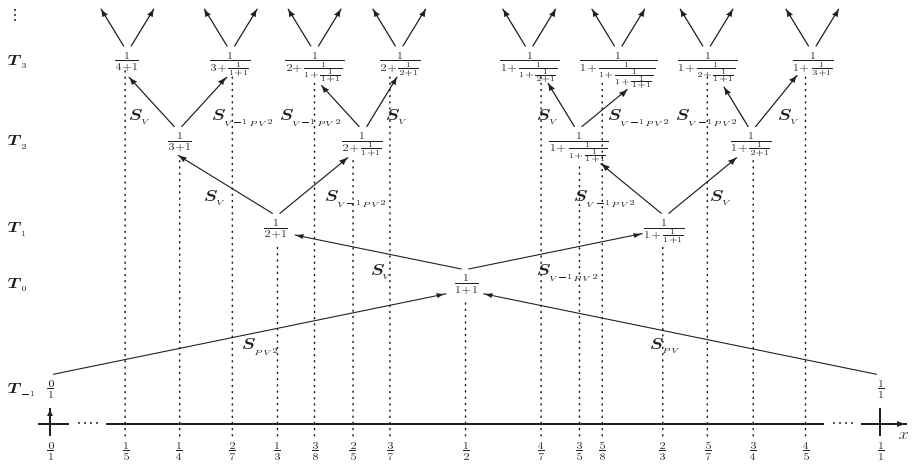

Figure 5: Binary "Farey graph" $\mathfrak{F}(V_n, \boldsymbol{E}_n)$. Every real number $\tau \in [0,1]$ corresponds uniquely to one path in $\mathfrak{F}(V_n, \boldsymbol{E}_n)$ or equivalently, to a binary address.

acts in the *reduced* Hilbert space $\ell_2(\mathcal{L}_1)$. One can show that in our case the new matrix elements $(\boldsymbol{\mathcal{H}}_{|\,\mathcal{M}}[z])_{\mu\nu} = (\boldsymbol{\mathcal{H}}[\boldsymbol{\epsilon}_{|\,\mathcal{M}}, \boldsymbol{t}_{|\,\mathcal{M}}])_{\mu\nu}$, with $\mu, \nu \in \mathcal{L}_1$, have the same tridiagonal structure as Eq. (5), but with the new, renormalized parameters $\boldsymbol{\epsilon}_{|\,\mathcal{M}}$ and $\boldsymbol{t}_{|\,\mathcal{M}}$, respectively. The latter are rational functions of the original parameters $\boldsymbol{\epsilon}$, $\boldsymbol{t}$, and the (complex) energy $z = E + i\eta$. For details see Refs. [17] and [18]. Suppose we start with the Hamiltonian $\hat{\boldsymbol{\mathcal{H}}}_{\Sigma}[\boldsymbol{\epsilon}, \boldsymbol{t}]$ associated with the dual word Σ, acting in the Hilbert space $\ell_2(\mathcal{L}) = \ell_2(\mathcal{L}_1) \oplus \ell_2(\mathcal{L}_2)$, then the correspondence

$$\boldsymbol{\mathcal{M}}(\Sigma') = \Sigma \quad \Longleftrightarrow {}^{R}\hat{\boldsymbol{\mathcal{M}}}^{-1} \cdot \hat{\boldsymbol{\mathcal{G}}}_{\Sigma}[\boldsymbol{\epsilon}, \boldsymbol{t}](z) = \hat{\boldsymbol{\mathcal{G}}}_{\Sigma'}[\boldsymbol{\epsilon}_{|\,\mathcal{M}}, \boldsymbol{t}_{|\,\mathcal{M}}](z) \tag{18}$$

is valid, where $\hat{\boldsymbol{\mathcal{G}}}_{\Sigma'}[\boldsymbol{\epsilon}_{|\,\mathcal{M}}, \boldsymbol{t}_{|\,\mathcal{M}}](z)$ acts in the Hilbert space $\ell_2(\mathcal{L}_1)$.

Omitting in the following the details of the construction of filtrations of Hilbert spaces and K–theory [17, 18], we now show the basic idea how to calculate the local density of states $\rho_\mu(E)$ for all sites μ. We will demonstrate the deep connection between path renormalization and spiky structures like in Fig. 4, where the LDOS $\rho_\mu(E) = |\Psi^+_\mu(E)|^2$ is plotted as a function of the site μ for two different energies E. The boundary conditions $\epsilon_{\mu+f_n} = \epsilon_\mu$, and $t_{\mu+f_n} = t_\mu$, respectively, immediately imply the relations

$${}^{R}\hat{\boldsymbol{\mathcal{T}}} \cdot \hat{\boldsymbol{\mathcal{G}}}_{\Sigma}(z) = \hat{\boldsymbol{\mathcal{G}}}_{\mathcal{T}(\Sigma)}(z) \quad \text{and} \quad {}^{R}\hat{\boldsymbol{\mathcal{T}}}(\rho_{\Sigma,\,\mu}) = \rho_{\mathcal{T}(\Sigma),\,\mu+1}, \tag{19}$$

and consequently

$$\rho_{\Sigma,\,\mu} = {}^{R}\hat{\boldsymbol{\mathcal{T}}}^{\mu}(\rho_{\Sigma,\,0}) = \frac{1}{\pi}\big(\Im\boldsymbol{m}\,\hat{\boldsymbol{\mathcal{G}}}_{\mathcal{T}^{\mu}(\Sigma)}(z)\big)_{00}. \tag{20}$$

Here ${}^{R}\hat{\boldsymbol{\mathcal{T}}}$ is the dual of the shift operator with the property $({}^{R}\hat{\boldsymbol{\mathcal{T}}}\psi)_\mu = \Psi_{\mu+1}$ for all μ, while we set $\boldsymbol{\mathcal{T}}(\Sigma) = (\sigma_1, \ldots, \sigma_p, \sigma_0)$ for every $\Sigma = (\sigma_0, \sigma_1, \ldots, \sigma_p)$. The main idea of path renormalization is the substitution of the shift operators ${}^{R}\hat{\boldsymbol{\mathcal{T}}}_\mu = {}^{R}\hat{\boldsymbol{\mathcal{T}}}^{\mu}$ with elementary substitutions

$\boldsymbol{\mathcal{M}}$. In Ref. [17] we constructed the orbit $\boldsymbol{\mathcal{O}}(\omega) \equiv \left\{ \boldsymbol{\mathcal{T}}^{\mu}(\omega) \,|\, \mu \in \mathbb{N} \right\}$ with

$$\left\{ \boldsymbol{\mathcal{T}}_{\mu} \,|\, \mu \in \mathbb{N} \right\} \cong \left\{ \boldsymbol{\mathcal{M}}^{(\mu)} \;\middle|\; \boldsymbol{\mathcal{M}}^{(\mu)} = \lim_{n_\mu \to \infty} \prod_{k_\mu=1}^{n_\mu} \boldsymbol{\mathcal{M}}'_{k_\mu,\bullet},\ \mu \in \mathbb{N} \right\},$$

$$\omega = \boldsymbol{\mathcal{M}}(L), \quad \boldsymbol{\mathcal{M}} := \lim_{n\to\infty} \prod_{k=1}^{n} \boldsymbol{\mathcal{M}}_k. \tag{21}$$

where $\boldsymbol{\mathcal{M}}'_{k_\mu,\bullet} \in \boldsymbol{\mathcal{A}}^{\Phi}$. $\boldsymbol{\mathcal{A}}^{\Phi}$ is an alphabet of elementary substitutions. In the case of the FC considered here we have $\boldsymbol{\mathcal{A}}^{\Phi} = \{\boldsymbol{\mathcal{L}}, \boldsymbol{\mathcal{R}}\}$ and $\boldsymbol{\mathcal{M}}_k = \boldsymbol{\mathcal{L}}$. The general case of generalized FC or arbitrary substitutions on n–letter alphabets (n finite) is investigated in Ref. [18]. For generalized Fibonacci words one can use $\boldsymbol{\mathcal{M}}_k = \boldsymbol{\mathcal{P}}\boldsymbol{\mathcal{V}}^{N_k}$, with $\boldsymbol{\mathcal{P}}(L,S) = (S,L)$ and $\boldsymbol{\mathcal{V}}^{N_k} = (\boldsymbol{\mathcal{P}}\boldsymbol{\mathcal{L}})^{N_k}$. The associated alphabet $\boldsymbol{\mathcal{A}}^{\Phi}$ is given in Ref. [17]. Fig. 5 shows all relevant possibilities of $\prod_k \boldsymbol{\mathcal{M}}_{N_k}$ and their connections to the angle α, defined in Fig. 1(a). This diagrams of this type are called "Farey graph" because it yields the well–known Farey construction of real numbers on the interval $[0,1]$. Their construction rules may be found in Refs. [21, 34]. Note, that in Fig. 5 we used the fact that $\boldsymbol{\mathcal{M}}_2\boldsymbol{\mathcal{M}}_1$ corresponds uniquely to $\boldsymbol{S}_{M_2}\boldsymbol{S}_{M_1}$. $S_M : \tau \to \tau'$ is the Möbius transformation corresponding to the substitution matrix $\boldsymbol{S}_{\mathcal{M}}$ which corresponds to the substitution $\boldsymbol{\mathcal{M}}$ [18].

The key message of Eq. 21 is, that it is always possible to find a succession of elementary substitutions for any $\mu \in \mathbb{N}$ (here $\boldsymbol{\mathcal{L}}$, and $\boldsymbol{\mathcal{R}}$ respectively), such that

$$\begin{aligned} \boldsymbol{\mathcal{M}}(L) = \omega \quad \Longleftrightarrow \quad \rho_{\Sigma,\,\mu}(E) &= \frac{1}{\pi}\Im\boldsymbol{m}\left(({}^{R}\hat{\boldsymbol{\mathcal{M}}}^{(\mu)})^{-1} \cdot \hat{\boldsymbol{\mathcal{G}}}_{\Sigma}[\boldsymbol{\epsilon},\boldsymbol{t}](z) \right)_{00} \\ &= \frac{1}{\pi}\Im\boldsymbol{m}\left(\hat{\boldsymbol{\mathcal{G}}}_{\alpha}[\boldsymbol{\epsilon}_{|\,\mathcal{M}^{(\mu)}}, \boldsymbol{t}_{|\,\mathcal{M}^{(\mu)}}](z) \right)_{00} \\ &= \frac{1}{\pi}\Im\boldsymbol{m}\,\frac{1}{\sqrt{(z-\epsilon_{\alpha|\,\mathcal{M}^{(\mu)}})^2 - 4t^2_{L|\,\mathcal{M}^{(\mu)}}}} \end{aligned} \tag{22}$$

with

$$({}^{R}\hat{\boldsymbol{\mathcal{M}}}^{(\mu)})^{-1} := \lim_{n_\mu\to\infty} \prod_{k_\mu=n_\mu}^{1} {}^{R}\hat{\boldsymbol{\mathcal{M}}}'^{\,-1}_{k_\mu,\bullet}, \tag{23}$$

where ${}^{R}\hat{\boldsymbol{\mathcal{M}}}'^{\,-1}_{k_\mu,\bullet}$ is the super operator corresponding to the deflation $\overline{\boldsymbol{\mathcal{M}}'_{k_\mu,\bullet}}^{-1}$. The last expression in Eq. (22) is the consequence of the underlaying periodic boundary conditions. From Eq. (22) one concludes that the LDOS is completely determined by the behaviour of the dynamical system

$$\begin{aligned} \left(\boldsymbol{\epsilon}_{|\,\mathcal{M}^{(\mu)}}, \boldsymbol{t}_{|\,\mathcal{M}^{(\mu)}}\right) &= ({}^{R}\boldsymbol{\mathcal{M}}^{(\mu)})^{-1}(\boldsymbol{\epsilon},\boldsymbol{t}), \\ \left(\boldsymbol{\epsilon}^{(k_\mu)}, \boldsymbol{t}^{(k_\mu)}\right) &= {}^{R}\boldsymbol{\mathcal{M}}'^{\,-1}_{k_\mu,\bullet}\left(\boldsymbol{\epsilon}^{(k_\mu-1)}, \boldsymbol{t}^{(k_\mu-1)}\right), \quad k_\mu = 1,2,\ldots,\infty, \end{aligned} \tag{24}$$

with $(\boldsymbol{\epsilon}^{(0)}, \boldsymbol{t}^{(0)}) = (\boldsymbol{\epsilon}, \boldsymbol{t})$.

Our approach has a nice geometrical interpretation. To find the concrete sequence for the super operators Eq. (23) one has to follow one of the corresponding paths in the associated

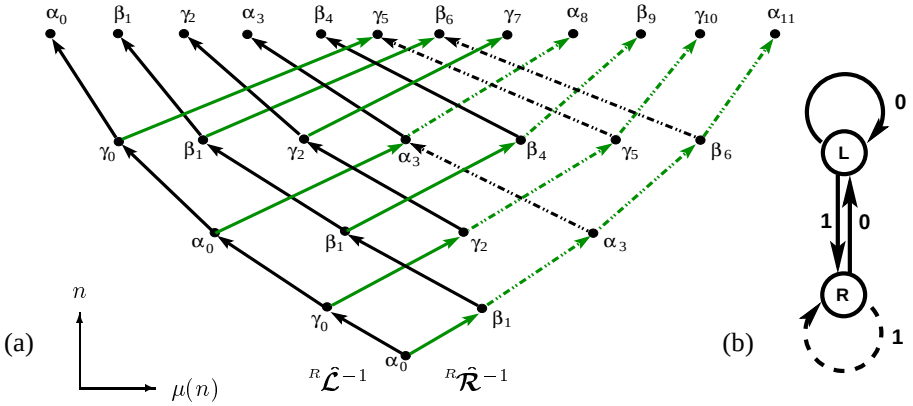

Figure 6: (a) The hierarchical graph $\mathfrak{G}^{\Gamma}(V,\boldsymbol{E})$ for the FC. To every directed edge (arrow) in the set $\boldsymbol{E}$ corresponds a super operator ${}^{R}\hat{\boldsymbol{\mathcal{M}}}'^{-1}_{k_\mu,\cdot}$. Arrows pointing to the left (resp. right) site correspond to ${}^{R}\hat{\boldsymbol{\mathcal{L}}}^{-1}$ (resp. ${}^{R}\hat{\boldsymbol{\mathcal{R}}}^{-1}$) associated to the deflations $\overline{\boldsymbol{\mathcal{L}}}^{-1}$ (resp. $\overline{\boldsymbol{\mathcal{R}}}^{-1}$). (b) To each graph $\mathfrak{G}^{\Gamma}(V,\boldsymbol{E})$ one can find a generating automaton [18].

hierarchical graph $\mathfrak{G}^{\Gamma}(V,\boldsymbol{E})$, first introduced in Ref. [17]. For the case of the FC we plot $\mathfrak{G}^{\Gamma}(V,\boldsymbol{E})$ in Fig. 6. Each directed line (arrow) $\boldsymbol{e} \in \boldsymbol{E}$ corresponds to a super operator. For $n = 1, 2, \ldots$ we assign the vertices $\sigma_{\mu(n)} \in V,\ \mu(n) = 0, 1, \ldots, p(n)$ with $p(n) = \max(\mu(n))$, and $\sigma \in \{\alpha, \beta, \gamma\}$ respectively, the LDOS $\rho_{\Sigma_n,\mu(n)}(E)$, where we have set $\Sigma_n = (\sigma_{0(n)}, \sigma_{1(n)}, \ldots \sigma_{p(n)})$. Details may be found in Refs. [17, 18].

C. Electrical Conductivity

In the linear response theory the real part of the conductivity is given by [35]

$$\Re e\{\sigma^{(n)}(\omega)\} = \frac{\pi}{\hbar}\int_{-\infty}^{\infty}\frac{f(E)-f(E+\hbar\omega)}{\hbar\omega}\,\Gamma^{(n)}(E,\omega)\,\mathrm{d}E\,, \tag{25}$$

$$\Gamma^{(n)}(E,\omega) = \mathbf{Tr}\big\{\hat{\boldsymbol{J}}\,\delta\big(E-\hat{\boldsymbol{\mathcal{H}}}_{\Sigma^{(n)}}\big)\hat{\boldsymbol{J}}\,\delta\big(E+\hbar\omega-\hat{\boldsymbol{\mathcal{H}}}_{\Sigma^{(n)}}\big)\big\}\,, \tag{26}$$

where $f(E)$ is the Fermi function and $\hat{\boldsymbol{J}}$ is the current operator

$$\hat{\boldsymbol{J}} = \frac{ie\hbar}{m}\sum_{\mu,\nu\in G} j_{\mu\nu}\,|\mu\rangle\langle\nu|, \quad j_{\mu\nu} = -t_{\mu_+}\delta_{\mu\nu-1} + t_{\mu_-}\delta_{\mu\nu+1}\,. \tag{27}$$

The frequency dependent electrical conductivity $\sigma(\omega)$ depends on the density of initial and final states as well as on the wave functions which determine the dipole matrix elements. In a recent article [26], we derived a suitable expression of Eq. (26) in terms of the known 2×2 transfer matrices and additional 5×5 matrices $\boldsymbol{\Delta}$, which allow us to set up a real–space renormalization scheme and its numerical implementation.

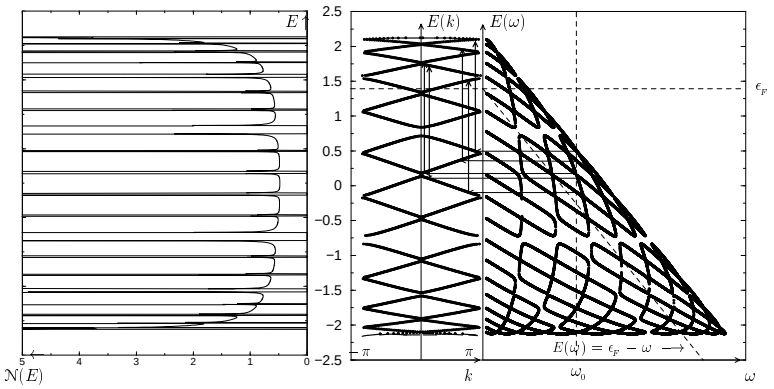

Figure 7: Density of states (left), bandstructure (middle), and (unrestricted) transition energies (wave number k may be real/imaginary) between the subbands (right) as function of frequency. 6^{th} order generation FC with $\epsilon_\alpha = \epsilon_\beta = \epsilon_\gamma = 0$ and $t_{_L} = 1.1,\ t_{_S} = 1.0$.

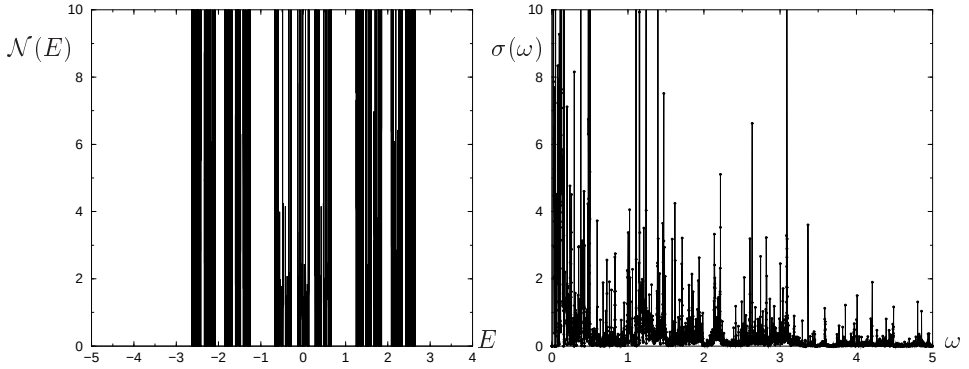

Figure 8: Density of states $\mathcal{N}^{(11)}(E)$ (left) and conductivity $\sigma^{(11)}(\omega)$ (right) of the FC with a supercell of $f_{11} = 233$ sites. Fermi energy $\epsilon_F = 0, t_S = 1.0, t_L = 1.5$, and $\epsilon_\alpha = \epsilon_\beta = \epsilon_\gamma = 0$ (arbitrary units).

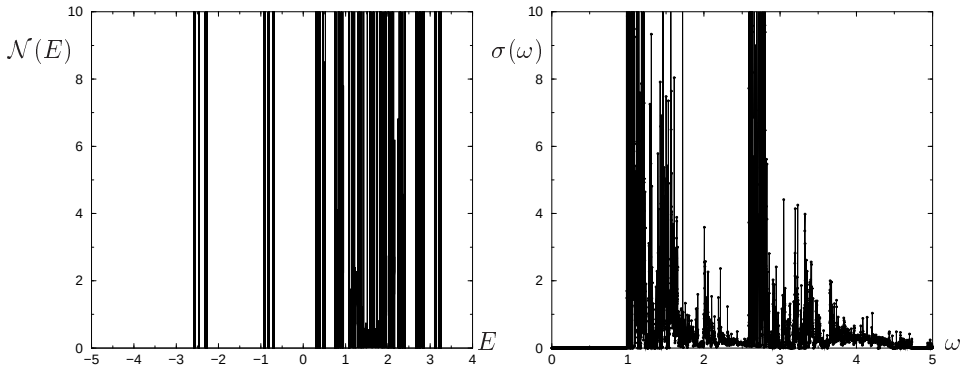

Figure 9: Density of states (left) and conductivity (right) of the same FC as in Fig. 8 but with different parameters: $\epsilon_F = -0.2$, $-\epsilon_\alpha = \epsilon_\beta = \epsilon_\gamma = 1.0$.

0.1.3 Results and Conclusion

The main challenge in the numerical evaluations turned out to be the calculation of the subband transition energies displayed in Fig. 9. This task implicitly implies the evaluation of polynomials of very high order. Such operations are numerically unstable, but could be managed with the help of Bailey's multiprecision software packet [36].

Figs. 7, 8, and 9 display some numerical results for the DOS, mini–band structure, transition energies, and the frequency dependent conductivity. For frequency $\omega \rightarrow 0$, merely $\sigma^{(n)}(0)$ contributes because none of the lines $(E_\omega^{(i)}, \omega)$ cut the axis $\omega = 0$ for energies *within* the energy spectrum. Therefore, $\sigma^{(n)}(\omega)$ vanishes in the limit $\omega \rightarrow 0$. Moreover, there is always a gap in the neighbourhood of $\omega = 0$. If one introduces some mechanism of dissipation or disorder, one may expect that the small gap in $\sigma(\omega)$ at $\omega = 0$ revealed in Fig. 8 may be smeared out (leading to metallic behaviour), but will persist in the case of Fig. 9 (semiconducting behaviour).

Starting from the self–similarity of the FC, we found a real space renormalization scheme for the Green's function as well as for the Kubo conductivity, which is suitable for numerical implementation. Hereto, these schemes stand alongside with the powerful tool of the trace map for the spectrum and the path renormalization scheme for the local DOS [17]. For details and generalizations of our approach to arbitrary morphisms (like Thue–Morse, Rudin–Shapiro, period doubling) and n-letter alphabets, we refer to Ref. [18].

0.2 Interaction–induced Correlations and Hume–Rothery Stabilization

The microscopic origin of the stability of quasicrystalline phases continues to be an unresolved issue. While at high temperatures the long-range order of quasicrystals and approximants may be favored over crystalline order because of entropic effects [15], striking interrelations between the ionic and the electronic structures [3, 11] especially in icosahedral (i) quasicrystals seem to indicate that electronic stabilization plays an important role at short and intermediate length scales of several atomic spacings: (1) The electron density of states (DOS) has a pronounced, structure-induced pseudogap at the Fermi level ε_F. (2) The position k_p of the main ionic structural peak coincides with twice the Fermi wave number, $2k_F \simeq k_p$ [12]. (3) In dependence of the composition from their constituents, quasicrystalline phases are only stable in small regions where the condition $2k_F \simeq k_p$ is satisfied. (4) In the quasicrystalline phase the electrical conductivity is substantially smaller than that of each of the elemental constituents. Similar coincidences between electronic and ionic structures are observed in amorphous noble-polyvalent alloys [12, 37]. These findings may be traced back to the common feature of these materials that the ion system exhibits concentrical, shell-like density correlations, where the spacing a between neighboring shells coincides with the Friedel wavelength, $\lambda_F \equiv \pi/k_F = 2\pi/k_p \equiv a$. Therefore, it has been conjectured that the electronic Friedel oscillations around an arbitrary central ion give an important contribution to the pair potential. As a consequence, the total energy of the system should be optimized by the ions effectively being bound in the minima of the Friedel potential and a concommittant pseudogap formation at ε_F. The importance of such a Hume-Rothery (HR) stabilization mechanism is supported

by detailed theoretical studies at temperature $T = 0$ both for amorphous [38] and for quasicrystalline [39, 40, 41, 42] systems. Numerical simulations [43] show that quasicrystalline structures can indeed be grown by the use of pair potentials with appropriate repulsive (i.e. oscillatory) parts.

However, at the relevant temperatures where quasicrystals or amorphous structures are stable ($T \simeq 10^2 \ldots 10^3 K$), regular Friedel oscillations are exponentially damped, and the thermal ion energy is so large that the experimentally observed short- to intermediate-range concentrical ion density correlations cannot be understood on the basis of the conventional Friedel oscillations alone.

In the present work it is shown that the interplay between Coulomb electron-electron interaction and disorder can lead to a strong enhancement as well as to a systematical phase shift of the Friedel oscillations even at finite T. Both effects compare well with available experimental results on amorphous HR alloys, and support the validity of the HR mechanism even at elevated temperatures.

0.2.1 Model and Effective Interaction

We now discuss an effective model for the electron motion in amorphous and quasicrystalline systems at $T > 0$. The ionic density correlations mentioned above constitute a scattering potential for the electrons whose scattering T-matrix $t_{\vec{k},\vec{k}'}$ is, by definition, proportional to the static ion structure factor, $t_{\vec{k},\vec{k}'} \propto S(|\vec{k} - \vec{k}'|)$, which in turn is peaked at a momentum transfer $q \equiv |\vec{k} - \vec{k}'| = k_p \simeq 2k_F$ and thus leads to enhanced backscattering. As has been shown [50, 51, 19], the latter not only generates a pseudogap but at the same time leads to a substantial increase of the electron transport or density relaxation rate, τ^{-1}, over the quasiparticle decay rate, τ_{qp}^{-1}. τ^{-1} is related to the conductivity σ by $\sigma = ne^2\tau/m^*$. Thus, $\tau^{-1} > \tau_{qp}^{-1}$ is a generic feature of the amorphous and the quasicrystalline state. In quasicrystals, when the conductivity is substantially reduced below the Drude result, we may have $\tau^{-1} \gg \tau_{qp}^{-1}$.

In addition, at the relevant, finite temperatures the phase coherence of the electrons is lost on the length scale of the inelastic mean free path. It follows that the electrons cannot probe the long-range order in a quasicrystal. Rather, they experience an effective potential made up of randomly placed, spatially extended scattering centers, each one characterized by the T-matrix $t_{\vec{k},\vec{k}'}$. For a detailed derivation of the effective disorder model see [44]. In such a random potential the electronic motion is diffusive instead of ballistic, similar as in amorphous metals. When the electron coherence length is long enough (low T), the motion may be subdiffusive with a diffusion exponent $\beta < 1/2$ [16, 45]. However, for the present purpose the precise value of β is unimportant, and we will assume $\beta = 1/2$ (classical diffusion) in the following.

Diffusion, as a dissipative process, is difficult to incorporate in an *ab initio* calculation. Therefore, we will choose a Feynman diagram technique, where diffusion arises by averaging over all (quasi-)random configurations of the system. In a diffusive electron sea screening is inhibited, so that the effective Coulomb interaction, $v_q^{eff}(z, Z)$, between electrons with complex frequencies z and $z + Z$ acquires a long-range, retarded part [46],

$$v_q^{eff}(z, Z) = \frac{v_q \Gamma^2(z, Z, q)}{\epsilon^{RPA}(Z, q)}, \quad v_q = \frac{4\pi e^2}{q^2}, \tag{28}$$

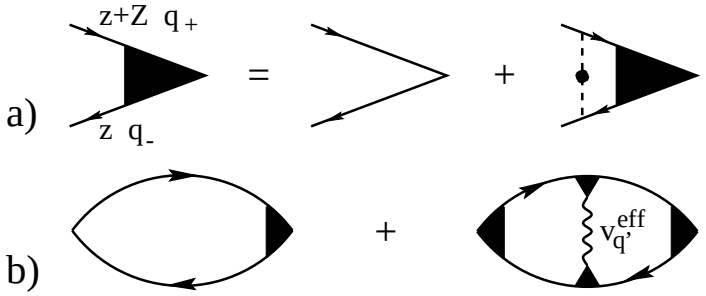

Figure 10: a) Diagrammatic definition of the diffusion vertex Γ. b) Polarisation $\Pi(0,q)$ including leading order quantum correction induced by disorder and interactions. Dashed lines denote electron–ion scattering T-matrix $t_{\vec{k},\vec{k}'}$, the wavy line with solid triangles the effective Coulomb interaction.

where $\epsilon^{RPA}(Z,q) = 1 + 2\pi i\,\sigma\,/(Z\,\mathrm{sgn}Z'' + iq^2 D)$ is the disordered RPA dynamical dielectric function, and the diffusion vertex, defined in Fig. 1 a), is

$$\Gamma(z,Z,q) = \begin{cases} \frac{i/\tau\ \mathrm{sgn}Z''}{Z + iq^2 D\ \mathrm{sgn}Z''} & z''(z+Z)'' < 0 \\ 1 & \text{otherwise.} \end{cases} \tag{29}$$

$D = 1/3\ v_F^2 \tau$ and $''$ denote the diffusion constant and the imaginary part, respectively, and $\beta = 1/2$. The long-range nature of v_q^{eff} is a consequence of the hydrodynamic ($Z, q \to 0$) pole of Γ, Eq. (2). Since diffusion is a classical phenomenon, guaranteed by particle number conservation, the form Eq. (1) of the effective interaction persists at finite T.

There are two experimental indications for the diffusion model of electron transport to be valid in i-quasicrystals. First, note that the diffusion-enhanced effective Coulomb interaction Eq. (1) implies the well-known $\sqrt{|E - \varepsilon_F|}$ dependence of the DOS in the pseudogap of disordered systems [46], where the half-integer power is characteristic for diffusion. The fact that a powerlaw dip in the DOS at ε_F with an exponent very close to 1/2 has been observed in i-quasicrystals by tunneling measurements [47] may be taken as an indication that the electron motion is indeed diffusive in these systems, and that the effective interaction has indeed the Alt'shuler-Aronov form Eqs. (1), (2). Second, the diffusion model, based on a finite phase coherence length, explains why the spikiness of the DOS, predicted for ideal quasicrystals at $T = 0$, has up to now not been observed experimentally [48].

0.2.2 Electron Density Response

The dynamical screening of the electron-electron interaction in a diffusive metal may be expected to drastically affect the screening charge distribution around an ion in the electron sea as well. In order to calculate this effect on the Friedel oscillations, we must consider the static charge density response $\chi(0,q)$ in the vicinity of $q = 2k_F$. It is given in terms of the polarization function $\Pi(0,q)$ as $\chi(0,q) = \Pi(0,q)/(1 - v_q \Pi(0,q))$. The first term of Fig. 1 b), $\Pi^{(0)}(0,q)$, corresponds to the well-known Lindhard function (RPA) [50]. In this diagram Γ contributes only a nonsingular factor of $O(1)$, since here the effective interaction v_q^{eff} enters in the static limit at wave numbers $q \simeq 2k_F$, where the diffusion vertex Γ is structureless.

We are thus led to consider quantum corrections where Γ gives contributions with vanishing frequency and momentum transfer, so that the *hydrodynamic* transport properties become important, although the response is taken at large external wave numbers q. The most singular contribution of this type arises from the quantum correction $\Pi^{(1)}(0,q)$, shown in Fig. 1 b), 2nd diagram.

While diffusive density relaxation occurs in general for large times, $t > \tau$, in $\Pi^{(1)}(0,q)$ it is, in addition, cut off for times larger than the life time τ_{qp} of the quasiparticles, which are interacting via $v_{q'}^{eff}$. Thus, the frequency transfer in this term extends over the nonvanishing (see above) range $\tau_{qp}^{-1} \leq |Z| \leq \tau^{-1}$. It may be evaluated explicitly as [44, 19],

$$\Pi^{(1)}(0,q) = -C\frac{2m^*k_F}{(2\pi\hbar)^2}\frac{\tau_{qp}/\tau - 1}{(\varepsilon_F\tau)^{7/2}} \times \tag{30}$$
$$\int_{-\varepsilon_F}^{\varepsilon_F} \mathrm{d}\nu \frac{1/(4T)}{\cosh^2\frac{\nu}{2T}} \frac{x-1}{[(x-1)^2 + (\frac{1}{4\sqrt{2\varepsilon_F}\tau_{qp}})^2]^{3/4}} ,$$

where $x = x(\nu) = (q/2k_F)/\sqrt{1+\nu/\varepsilon_F}$ and C is a numerical constant of $O(1)$. It is seen that for $T = 0$, $\tau_{qp}^{-1} \to 0$ $\Pi^{(1)}(0,q)$ exhibits a powerlaw divergence $\propto -\mathrm{sgn}(q-2k_F)/|q-2k_F|^{1/2}$ at $q = 2k_F$. Although at finite T or τ_{qp}^{-1} the divergence of $\Pi^{(1)}(0,q)$ is reduced to a peak, the inverse dielectric function, $1/\varepsilon(q) = 1/(1 - v_q\Pi(0,q))$, still has a $q = 2k_F$ divergence at a critical transport rate, $\tau_c^{-1}(T)$ because of the vanishing denominator. This leads to a systematical enhancement as well as to a phase shift of the Friedel oscillations (see below). On the other hand, when there is no enhanced backscattering, we have $\tau_{qp}/\tau = 1$, and the peak structure of $\Pi(0,q)$ vanishes. Eq. (3) constitutes an extension of previous work [19] in that the finite quasiparticle life time is explicitly taken into account. The parameter τ^{-1} may be varied by changing the composition of the alloy.

0.2.3 Comparison with Experiments

In the following, the theory summarized in the previous section is applied in the region $1/\varepsilon_F\tau_{qp} \ll 1$ to a large class of noble-polyvalent metal alloys like $Cu_{1-x}Sn_x$. We restrict ourselves to the comparison with amorphous phases here, because of their structural similarities to QC systems, and because at the same time in the amorphous state the Fermi momentum can be varied over a wider range than in QCs. These HR alloys exhibit an amorphous to crystalline transformation (CAT) as a function of the composition of the alloy, and the thermal stability may be continuously varied. Remarkably, in all these systems (1) the thermal stability reaches a maximum at or near the CAT (Fig. 2) [37], and (2), assuming that the ions sit in the minima of the Friedel potential, the measured ionic positions suggest that there is a systematical phase shift φ of the Friedel oscillations [37], $\rho(r) \propto cos(2k_Fr - \varphi)$, with $\varphi = \pi/2$ at the CAT (inset of Fig. 2).

Fourier transforming $1 - 1/\varepsilon(q)$ to obtain $\rho(r)$ [50] shows that for incomplete Fermi surface-Jones zone matching, i.e. small $\tau^{-1} \simeq \tau_{qp}^{-1}$, the quantum corrections generate density oscillations $\rho^{(1)}(r) \propto -\cos(2k_Fr)/r^3$, which overcompensate the conventional Friedel oscillations, implying a phase shift of $\varphi = \pi$ [19]. As $\tau^{-1} \to \tau_c^{-1}$, the increasing $2k_F$ peak of $1/\varepsilon(q)$ leads, in addition, to density oscillations $\rho^{(1)}(r) \propto \sin(2k_Fr)/r^2$ [49], so that in

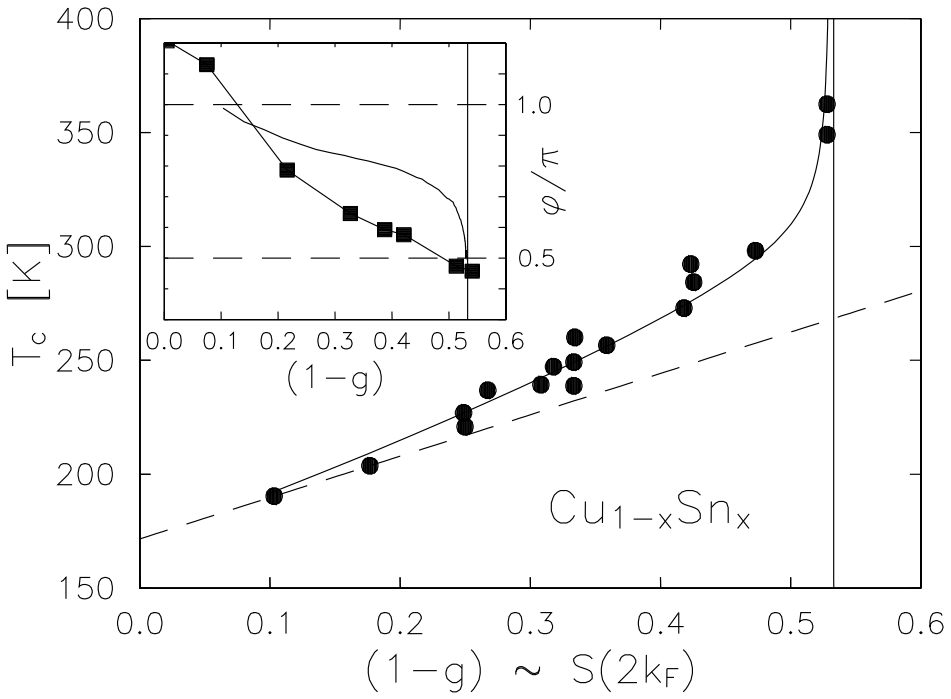

Figure 11: Crystallization temperature T_c as a function of the DOS suppression at ε_F, $(1-g)$. Data points represent T_c for a-$Cu_{1-x}Sn_x$ [5]. The solid curve is the fit of the present theory (see text). Vertical line: position of CAT. The inset shows the phase shift φ of the first maximum of the charge density distribution $\rho(r)$. Solid line: theory. Data points with solid line: measurements [5] for a-$Cu_{1-x}Sn_x$.

the vicinity of τ_c^{-1}

$$\rho(r) \propto -\frac{\cos(2k_F r)}{(2k_F r)^3} + A(\tau^{-1})\frac{\sin(2k_F r)}{(2k_F r)^2}, \tag{31}$$

with $A(\tau^{-1}) \simeq 0.343\pi(1-\tau^{-1}/\tau_c^{-1})^{-1/2}$. The exponent $1/2$ is characteristic for diffusive behavior. Thus, the Friedel oscillations are shifted by $\varphi = \pi - \tan^{-1}[2k_F r\ A(\tau^{-1})] \simeq \pi/2 + 1/(2k_F r A)$, i.e. the diverging Friedel amplitude necessarily goes hand in hand with $\varphi \to \pi/2 + 0$. Note that, in contrast to the conventional Friedel oscillations, this divergence is robust against damping due to finite T or disorder. The point where the amplitude, A, diverges should be identified with the CAT, since at this point the fluctuations of the Friedel potential also diverge, allowing the system to find its crystalline ground state. This process explains in a natural way the observed composition dependence of the thermal stability and of the phase shift φ mentioned at the beginning of this section.

For a direct comparison with experiments the control parameter of the theory, τ^{-1}, must be translated into a parameter which is experimentally accessible: It follows from the scattering theory [51, 19] that $\tau^{-1} = \tau_o^{-1} + \gamma\ S(2k_F)$, where the peak of the ionic structure factor,

$S(q = 2k_F)$, controls the backscattering amplitude, γ is a constant, and τ_o^{-1} is an offset due to momentum independent scattering. $S(2k_F)$ in turn is proportional [37] to the measured, structure–induced suppression of the DOS $N(\varepsilon_F)$ at the Fermi level, $1 - N(\varepsilon_F)/N_o(\varepsilon_F) \equiv 1 - g$, compared to the free electron gas, $N_o(\varepsilon_F)$. The resulting fit of the crystallization temperature, T_c, is shown in Fig. 2, where the contribution to the stability coming from the pseudogap formation is assumed to be linear in $(1 - g)$ (dashed line). The characteristic increase of T_c at the CAT, explained by the present theory, is clearly seen. The inset shows the calculated phase shift, φ, and the measured shift of the atomic nearest neighbor position relative to the position of the first conventional Friedel minimum, $a_o = \pi/k_F$. Note that there is no adjustable parameter in φ, once the fit of T_c has been performed. The overall behavior of the shift is well explained by the theory; however, the experimental data approaches $\varphi = \pi/2$ faster than predicted. The latter may be attributed to the fact that, as seen from the discussion after Eq. (31), the higher–order Friedel minima approach $\varphi = \pi/2$ faster than the first one. In this light, the agreement between theory and experiment is remarkably good.

0.2.4 Conclusion

The structural similarities [3] between amorphous alloys and *i*–quasicrystals suggest that the quantum effect discussed above may be important in the latter systems as well. In fact, quasicrystals seem to fulfill all the necessary conditions for this effect to occur, i.e. effectively diffusive electron motion [16, 45] and $\tau^{-1} \gg \tau_{qp}^{-1}$. The latter is supported by the Fermi surface matching, i.e. by the experimental observation [47] and theoretical prediction [39, 40, 41] of structure-induced pseudogaps. Moreover, another more commonly known effect of disorder–enhanced Coulomb interaction, the $\sqrt{|E - \varepsilon_F|}$ dependence of the DOS in the pseudogap [46], may have been already observed in *i*-quasicrystals by tunneling measurements of the DOS [47].

In conclusion, we have shown that the Friedel oscillations are enhanced by Coulomb interaction in the presence of disorder and enhanced backscattering. The results are relevant for the stability of amorphous and quasicrystalline metals. A selfconsistent formulation, treating the coupled electron and ion systems on equal footing within a continuum model, has been developed in Ref. [44]. It is proposed to include the enhanced Friedel potential calculated in the present work in the pseudopotential of more quantitative *ab initio* calculations.

0.3 Acknowledgments

Discussions with N. Ashcroft, R. Haberkern, P. Häussler, T. Kopp, P. Wölfle, and E. S. Zijlstra are gratefully acknowledged. This work was supported by the Deutsche Forschungsgemeinschaft through Schwerpunktprogramm “Quasikristalle”. J.K. is grateful for the hospitality of the ITP, University of California at Santa Barbara. The work of J.K. at ITP was supported in part by the National Science Foundation under Grant No. PHY99-07949.

Bibliography

[1] D. Shechtman, I. Blech, D. Gratias, and J. W. Cahn, Phys. Rev. Lett. **53**, 1951 (1984).

[2] C. Janot *Quasicrystals: A Primer*, (Clarendon Press, 1994).

[3] S. J. Poon, Adv. Phys. **41**, 303 (1992).

[4] F. Hippert and D. Gratias, Eds., *Lectures on Quasicrystals*, *Les Éditions de Physique*, (Les Ulis, France, 1994); Z. M. Stadnik, Ed., *Physical Properties of Quasicrystals*, Springer Series in Solid State Sciences **126** (Springer, 1999).

[5] *Proceedings of the 7th International Conference on Quasicrystals ICQ7*. F. Gähler, P. Kramer, H.–R Trebin, K. Urban eds. Mat. Sci. Eng. A **294**–**296** (Elsevier, 2000); *Proceedings of the 8th International Conference on Quasicrystals ICQ8*, to be published.

[6] S. E. Burkov, T. Timusk, and N. W. Ashcroft, J. Phys. Cond. Matter **4**, 9447 (1992).

[7] D. N. Basov, F. S. Pierce, P. Volkov, S. J. Poon, and T. Timusk, Phys. Rev. Lett. **73**, 1865 (1994).

[8] T. Fujiwara, Phys. Rev. B **40**, 942 (1989); J. Hafner and M. Krajčí, Phys. Rev. B **47**, 11 (1993); T. Fujiwara, S. Yamamoto, and G. T. de Laissardière, Phys. Rev. Lett. **71**, 4166 (1993); D. Mayou, C. Berger, F. Cyrot–Lackmann, T. Klein, and P. Lanco, Phys. Rev. Lett. **70**, 3915 (1993).

[9] Z. M. Stadnik *et al.*, Phys. Rev. B **64**, 214202 (2001).

[10] E. S. Zijlstra and T. Janssen, Europhys. Lett. **52**, 578 (2000); Phys. Rev. B **61**, 3377 (2000).

[11] R. Haberkern, K. Khedhri, C. Madel, and P. Häussler, Mat. Sci Eng. A **294**–**296**, 475 (2000).

[12] C. Madel, G. Schwalbe, R. Haberkern, and P. Häussler, Mat. Sci. Eng. A **294**–**296**, 535 (2000).

[13] K. Saitoh *et al.*, Jap. J. Appl. Phys. **36**, L1404 (1998); Y. Yan, S. J. Pennycook, and A. P. Tsai, Phys. Rev. Lett. **81**, 5145 (1998).

[14] W. Hume–Rothery, *The Metallic State* (Oxford University Press, New York, 1931).

[15] D. Joseph and V. Elser, Phys. Rev. Lett. **79**, 1066 (1997).

[16] J. Bellissard and H. Schulz–Baldes, J. Stat. Phys. **99**, 587 (2000); H. Schulz–Baldes and J. Bellissard, J. Stat. Phys. **91**, 991 (1998); Rev. Math. Phys. **10**, 1 (1998).

[17] D. Walther and R. v. Baltz, Phys. Rev. B **55**, 8852 (1997).

[18] D. Walther, Dissertation, Fakultät für Physik, Universität Karlsruhe, unpub. (Feb. 2003).

[19] J. Kroha, A. Huck, and T. Kopp, Phys. Rev. Lett. **75**, 4278 (1995).

[20] J. Kroha, Mat. Sci. Eng. A **294**–**296**, 500 (2000).

[21] K. Iguchi, Phys. Rev. B **43**, 5915 (1991); **43**, 5919 (1991).

[22] P. Kramer, J. Phys. A: Math. Gen. **26**, 213 (1993).

[23] M. Baake, U. Grimm, and D. Joseph, Int. J. Mod. Phys. B **7**, 1527 (1993).

[24] J. Nielsen, Math. Ann. **78**, 385 (1918), **91**, 169 (1924).

[25] D. Walther and R. v Baltz, in: *Aperiodic '97*, Proceedings of the International Conference on Aperiodic Crystals, Alpe d'Huez / Grenoble, Frankreich, (World Scientific, Singapore, 1998).

[26] D. Walther and R. v. Baltz, Journ. Low Temp. Phys **126**, 1211 (2002).
[27] B. Iochum and D. Testard, J. Stat. Phys. **65**, 715 (1991),
W. Salejda and P. Szyszuk, Physica A **252**, 547 (1998),
B. Sutherland and M. Kohmoto, Phys. Rev. **36**, 5877 (1987).
[28] S.I. Ben–Abraham and A. Joseph, *Proceedings of the 5th Int. Conf. on Quasicrystals*, eds. C. Janot and R. Mosseri, p. 621, (World Scientific, Singapore, 1995),
A. Lahiri, Phys. Rev.B **53**, 3702 (1996),
S. Roche and D. Mayou, Phys. Rev. Lett. **79**, 2518 (1997).
[29] W. Salejda und P. Szyszuk, Physica A **252**, 547 (1998).
[30] Leonardo Pisano (1170–1250), (named *Fibonacci*, from *filius Bonacci*), *Liber abbaci* (1202). For a historical review see: http://www–groups.dcs.st–and.ac.uk/~history/Mathematicians/Fibonacci.html
[31] C. Brezinski, *Padé–Type Approximation and General Orthogonal Polynominals.*, (Birkhäuser–Verlag, 1980).
[32] H. Weyl, Ann. Math. **68**, 220 (1910); E.C. Titchmarsh: *Eigenfunction Expansions Associated with Second–Order Differential Equations*, (Oxford, University Press, 1946).
[33] Natl. Bur. Stand. Appl. Math. Ser. No 55, edited by M. Abramowitz and I.A. Stegun, (U.S. GPO, Washington, DC) *Handbook of Mathematical Functions*, (Dover, 1968).
[34] P. Cvitanović, J. Myrheim, Commun. Math. Phys. **121**, 225 (1989); P. Cvitanović in *From Number Theory to Physics*, (Springer, 1992); J. M. Luck, C. Godréche, A. Janner, and T. Janssen, J. Phys. **A 26**, 1951 (1993).
[35] A. Douglas Stone und A. Szafer, IBM J. Dev., **32**, 384 (1988); H. U. Baranger und A.D. Stone, Phys. Rev. B **40**, 8169 (1989).
[36] D.H. Bailey, *Multiprecision Translation and Execution of Fortran Programs*, ACM Transactions on Mathematical Software, **19**, no. 3, Sept. 1993, p. 288-319.
[37] For a review and references see P. Häussler, Phys. Rep. **222**, 65 (1992).
[38] W. Jank and J. Hafner, Phys. Rev. B **41**, 1497 (1990).
[39] A. P. Smith and N. W. Ashcroft, Phys. Rev. Lett. **59**, 1365 (1987).
[40] T. Fujiwara and T. Yokokawa, Phys. Rev. Lett. **66**, 333 (1991).
[41] J. Hafner and M. Krajčí, Phys. Rev. Lett. **68**, 2321 (1992); M. Krajčí et al., Phys. Rev. B **51**, 17355 (1995); M. Krajčí, J. Hafner, and M. Mihalcovič, Phys. Rev. B **55**, 843 (1997).
[42] E. Cockayne and M. Widom, Phys. Rev. Lett. **81**, 598 (1998).
[43] V. E. Dmitrienko and S. B. Astaf'ev, Phys. Rev. Lett. **75**, 1538 (1995); V. E. Dmitrienko, S. B. Astaf'ev, and M. Kléman, Phys. Rev. B **59**, 286 (1999).
[44] J. Kroha, Habiliationsschrift (2001), to be published.
[45] F. Piéchon, Phys. Rev. Lett. **76**, 4372 (1996).
[46] B. L. Al'tshuler and A. G. Aronov, Solid State Commun. **30**, 115 (1979); B. L. Al'tshuler et al., Phys. Rev. B **22**, 5142(1980).
[47] D. N. Davydov et al., Phys. Rev. Lett. **77**, 3173 (1996); **74** (1995) 3656; T. Schaub et al., J. Non-Cryst. Sol. **250-252**, 874 (1999); J. Delahaye et al., *ibid.* 878 (1999).
[48] Z. M. Stadnik et al. Phys. Rev. Lett. **77**, 1777 (1996); Z. M. Stadnik, Mat. Sci. Eng. A **294**–**296**, 470 (2000).
[49] J. Kroha, A.Huck, and T. Kopp, Czech. J. Phys. **46**, 2275 (1996).
[50] G. D. Mahan, *Many Particle Physics*, (Plenum Press, New York 1990).
[51] J. Kroha, Physica A **167**, 231 (1990).